IEEE TRANSACTIONS ON
TRANSPORTATION
ELECTRIFICATION

IEEE Xplore® Digital Library
http://ieeexplore.ieee.org/Xplore

Comprehensive Analyses and Comparison of 1kW Isolated DC-DC Converters for Bidirectional EV Charging Systems

Peiwen He, *Student Member, IEEE*, and Alireza Khaligh, *Senior Member, IEEE*

***Abstract*—Isolated DC-DC converters with galvanic isolation are commonly used in electric vehicle (EV) battery chargers. These converters interface between a DC voltage link, which is usually the output of a power factor correction (PFC) stage, and an energy storage unit. CLLC and Dual Active Bridge (DAB) DC-DC converters can achieve high power density, high energy efficiency, wide gain range, galvanic isolation and bidirectional power flow, and therefore, have potential applications as DC-DC converters for bidirectional EV charging systems. In this manuscript, full-bridge CLLC (FBCLLC), half-bridge CLLC (HBCLLC), full-bridge DAB (FBDAB), and half-bridge DAB (HBDAB) DC-DC converters are evaluated and compared for their suitability for EV chargers. All the converters are designed with optimal soft-switching features. The operating principles, design methodologies and design considerations are presented. Prototypes of the converters with power rating of 1 kW are designed and developed. The prototypes interface a 500 V DC link and a 200 – 420 V load, which is common for electric vehicle applications. The performances of the circuits are analyzed and a comprehensive comparison is conducted.**

***Index Terms*—bidirectional, battery charger, CLLC, dual active bridge, isolated DC-DC converter, resonant converter, zero current switching (ZCS), zero voltage switching (ZVS).**

I. Introduction

THE concerns about global climate change and fossil fuel depletion are promoting the growth of electric vehicle (EV) market [1]. Researchers have studied various techniques to improve efficiency and power density of EV chargers [2]-[4]. A typical EV charger consists of an AC-DC power factor correction (PFC) stage and a galvanically isolated DC-DC converter [5]. The PFC stage, such as an interleaved boost converter, interfaces between the AC grid and a DC voltage link to achieve input PFC and AC to DC conversion [6] [7]. The DC-DC stage connects between the DC voltage link and an energy storage system [8].

For unidirectional grid-to-vehicle (G2V) chargers, LLC converters are commonly selected as the DC-DC stages [9] [10]. Recent studies indicate that EVs can also be considered as distributed power sources to store and send power back to the grid [11] [12]. This vehicle-to-grid (V2G) concept allows EVs to provide voltage and frequency regulation to the grid, absorb excess electricity and deliver it to the grid during periods of high demand. The V2G capability requires EVs to have bidirectional charging systems which are able to operate in two power flow modes: charging mode (G2V) and discharging mode (V2G). The CLLC and dual active bridge (DAB) converters are commonly used as the DC-DC stages for bidirectional EV chargers, due to their advantages in terms of high power density, high efficiency, buck/boost capability, and controllable bidirectional power transfer [13]-[15].

Both CLLC and DAB circuits can be designed with full-bridge and half-bridge topologies. Different topologies require different design methods and are appropriate for different applications. A bidirectional full-bridge CLLC (FBCLLC) converter, illustrated in Fig. 1(a), is introduced in [16]. The converter is proposed for a 500 W power rating, 400 V input and 48 V output UPS system, and possesses zero voltage switching (ZVS) and zero current switching (ZCS) features to minimize switching loss. The highest efficiency of the prototype is exceeding 96%. In [17], a design methodology for a 5 kW FBCLLC converter with soft start control is presented. The prototype is proposed for a 380 V DC power distribution system and the highest efficiency is 97.8% at 4 kW. A CLLC-compensated capacitive power transfer system for electric vehicle charging applications is proposed in [18]. The power rating of the system is 2.9 kW and the efficiency is 89.3%. Basic operating principles and simulation results of a half-bridge CLLC (HBCLLC) converter (shown in Fig. 1(b)) are reported in [19] without providing detailed experimental verification.

Fig. 2(a) illustrates the topology of a full-bridge DAB (FBDAB) converter. Detailed operating principles, design considerations and control method for a 10 kW FBDAB converter are discussed in [20]. Authors in [21] presents a design of a 5 kW prototype FBDAB converter for a 380 V input and 20-28 V output charger for a UPS system. The highest efficiency of this converter exceeds 96%. An analysis of switching condition and loss modeling of GaN-based DAB converter for EV charger is provided in [22], the modeling is verified by experimental measurement of a 500 kHz GaN DAB converter. A half-bridge DAB (HBDAB) converter (illustrated in Fig. 2(b)) for EV on-board charger is introduced in [23], and a 600 W prototype converter is built to verify the theoretical analysis and control method. By analyzing the optimal

P. He and A. Khaligh are with the Electrical and Computer Engineering Department and the Institute for Systems Research, University of Maryland, College Park, MD 20742 USA (e-mail: phe@umd.edu; khaligh@ece.umd.edu).

Digital Object Identifier: 10.1109/TTE.2016.2630927

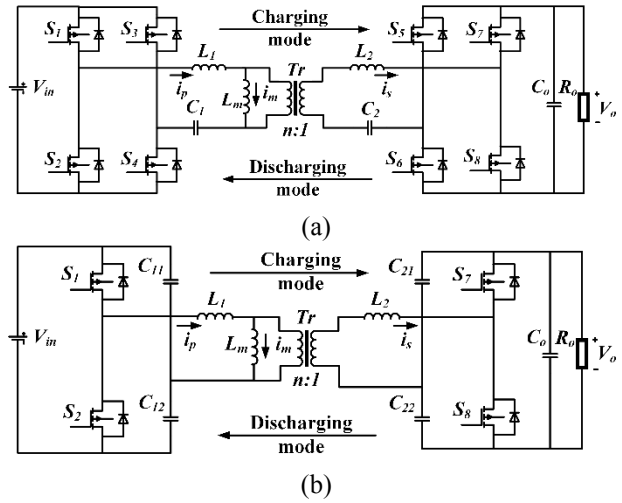

Fig. 1. Bidirectional (a) FBCLLC and (b) HBCLLC resonant converters.

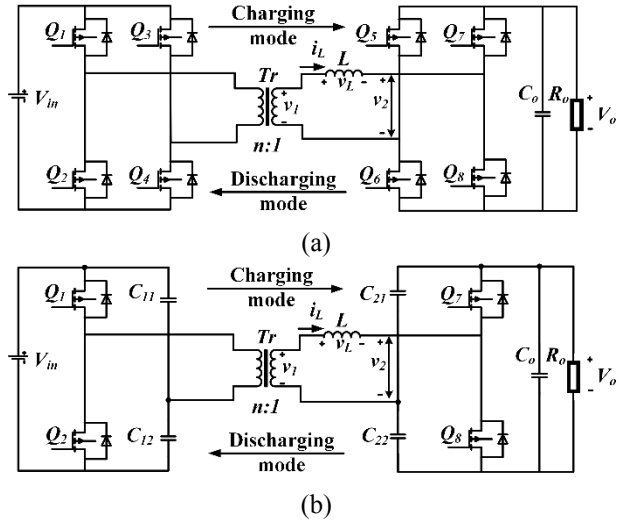

Fig. 2. Bidirectional (a) FBDAB and (b) HBDAB resonant converters.

operation regions of both FBDAB and HBDAB converters, [24] proposes a combined circuit which is able to switch between FBDAB and HBDAB to achieve high efficiency for wide load. This is verified by an 800 W prototype and the maximum measured efficiencies are 92.9% at light load and 93.4% at full load.

Frequency modulation is the basic control method for both FBCLLC and HBCLLC circuits. For FBDAB circuits, various control strategies, such as single-phase-shift (SPS), extended-phase-shift (EPS), dual-phase-shift (DPS), and triple-phase-shift (TPS) controls, can be applied through manipulating the on/off status of the switches on both primary and secondary sides of the converters [25]-[27]. For a HBDAB circuit, which consists of four switches, only SPS control method can be applied. However, the half-bridge topology has benefits in terms of reduced size, weight and cost, due to the reduction of the switches, corresponding driving circuits, and cooling systems. Therefore, it is necessary to discuss the advantages and disadvantages of the different topologies. In this manuscript, four DC-DC converter topologies, FBCLLC, HBCLLC, FBDAB, and HBDAB, are analyzed. The design methods of these four topologies for EV charging systems are introduced, and 1 kW prototypes for each topology are built to validate the analysis and designs. An important contribution of this manuscript is providing a general gain expression of the HBCLLC converter, analyzing and verifying the practicability of the four isolated DC-DC converters for bidirectional EV charging systems.

This manuscript organized as follows. The DC-DC converter topologies and their operating principles are discussed in Section II. Detailed design methodologies and considerations for EV charging systems are discussed in Section III. The experimental results are presented in Section IV and the analysis of the results are provided in Section V. Finally, Section VI provides the conclusion remarks.

II. Theoretical Analysis

CLLC and DAB converters are isolated switching converters. In order to ensure higher efficiency, the circuits need to be designed to operate under soft-switching conditions. In the case of CLLC converters, ZVS operation can be achieved on primary side power MOSFETs and ZCS operation can be realized on secondary side rectifiers. In the case of DAB converters, both primary and secondary side power MOSFETs can operate under ZVS condition.

A. Bidirectional CLLC converters

1) Operating Principles

The bidirectional CLLC converters have symmetrical structures consisting of primary inverting stages and secondary rectifying stages. For the FBCLLC circuit (shown in Fig. 1(a)), L_1 and L_2 are resonant inductors, C_1 and C_2 are resonant capacitors. In comparison, the HBCLLC circuit (shown in Fig. 1(b)) uses bridge capacitors (C_{11}, C_{12}, C_{21}, and C_{22}) as resonant capacitors. The turns ratio of the transformer Tr is n: 1, and its magnetizing inductance is L_m. Fig. 3 illustrates typical waveforms of a bidirectional FBCLLC or HBCLLC circuit operating at a switching frequency lower than its resonant frequency. The dead band duration is the time between t_a and t_b, where all the switches are off to prevent the bridges from short-circuit shoot-through. In this interval, no power transfers to the secondary side, and the secondary side resonant inductor current, i_s, is zero. At time t_b, the gate voltages, v_{s1} and v_{s2} (only v_{s1} for the HBCLLC circuit) are applied. The primary side resonant inductor current, i_p, is negative, which means the current freewheels through the body diodes of S_1 and S_4 (only S_1 for the HBCLLC circuit), therefore S_1 and S_4 (only S_1 for the HBCLLC circuit) will turn on with ZVS at t_1. Beyond t_b, power transfers from the primary side to the secondary side through the transformer and i_s is positive. Between t_b and t_c, i_p resonates and the magnetizing inductance current, i_m, keeps increasing almost linearly, since L_m is much larger than L_1. When i_p meets i_m at t_c, previous resonance stops, and no power transfers to the secondary side, hence i_s becomes zero. The body diodes of S_6 and S_7 (only S_7 for the HBCLLC circuit) will turn off with ZCS naturally. The other half cycle has similar

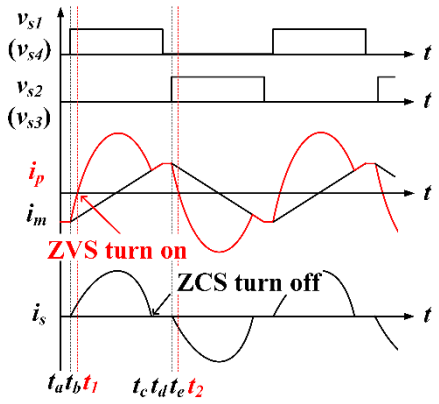

Fig. 3. Typical waveforms of a bidirectional FBCLLC or HBCLLC converter operating at a frequency lower than resonant frequency.

operating mode but with opposite current direction.

2) Gain Analysis

The equivalent circuits of the FBCLLC converter and HBCLLC converter for charging mode are shown in Fig. 4(a) and (b), respectively. R_e, L_2', and C_2' are the equivalent R_o, L_2, and C_2 of the converters, respectively.

The general transfer function $H(s)$ of CLLC converters can be derived as follows:

$$H(s) = \frac{1}{n} \cdot \frac{R_e}{R_e + Z_{L2}' + Z_{C2}'} \cdot \frac{(R_e + Z_{L2}' + Z_{C2}') \| Z_{Lm}}{Z_{L1} + Z_{C_1} + (R_e + Z_{L2}' + Z_{C2}') \| Z_{Lm}} \tag{1}$$

The gain of the FBCLLC converter can be calculated as

$$G_{CLLC,G2V} = |H(s)| = \left|\frac{V_{out}}{V_{in}}\right| = \frac{1}{n} \cdot \frac{1}{\sqrt{a^2 + b^2}} \tag{2}$$

where,

$$a = \frac{1}{h} + 1 - \frac{1}{h \cdot \omega^2} \tag{3}$$

$$b = \left(\frac{k}{h} + 1 + \frac{1}{g \cdot h} + \frac{1}{g}\right)\frac{Q}{\omega} - \left(\frac{k}{h} + 1 + k\right)Q \cdot \omega - \frac{Q}{g \cdot h \cdot \omega^3} \tag{4}$$

$$\begin{cases} h = \frac{L_m}{L_1}, k = \frac{L_2'}{L_1}, g = \frac{C_2'}{C_1}, \omega = \frac{\omega_s}{\omega_r} \\ \omega_r = \frac{1}{\sqrt{L_1 C_1}}, Q = \frac{\sqrt{L_1/C_1}}{R_e} \end{cases} \tag{5}$$

ω_r and ω_s are the resonant frequency and operating frequency, respectively. ω is the normalized frequency, and Q is the quality factor. The First Harmonic Approximation (FHA) is applied to calculate the equivalent load. For FBCLLC circuit, the equivalent load, inductance, and capacitance can be calculated as:

$$R_{e,FB} = (8n^2/\pi^2)R_o \quad L_2' = n^2 L_2 \quad C_2' = C_2/n^2 \tag{6}$$

Similarly, for HBCLLC circuit, they are derived as follows:

$$\begin{aligned} R_{e,HB} &= (2n^2/\pi^2)R_o \quad & L_2' &= n^2 L_2 \quad & C_1 &= C_{11} + C_{12} \\ C_2' &= C_{21}' + C_{22}' \quad & C_{21}' &= C_{21}/n^2 \quad & C_{22}' &= C_{22}/n^2 \end{aligned} \tag{7}$$

Fig. 5 shows the gain curves versus normalized frequency at different loads. The gain increases, but the slope of the curve decreases with a lower Q. To simplify the design, for both FBCLLC and HBCLLC converters, k and g are set to be 1,

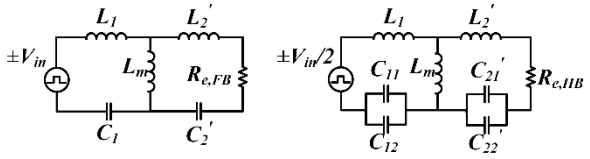

Fig. 4. Equivalent circuits of (a) the FBCLLC and (b) the HBCLLC converters in charging mode.

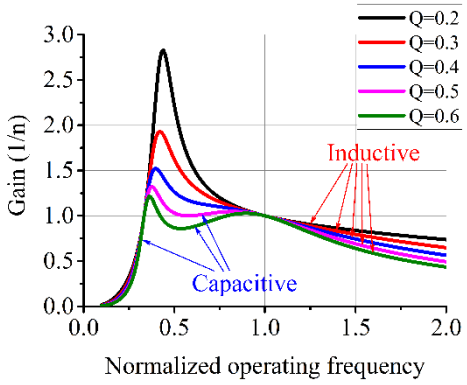

Fig. 5. Gain curves versus normalized frequency of CLLC converters at different loads.

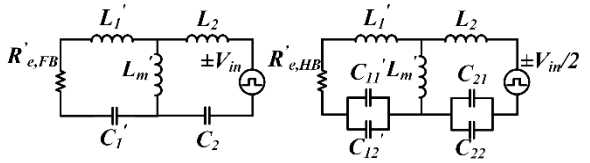

Fig. 6. Equivalent circuits of (a) the FBCLLC and (b) the HBCLLC converters in discharging mode.

which means $L_1 = L_2'$ and $C_1 = C_2'$, and h is set to be 4.

In discharging mode, the equivalent circuits of the FBCLLC converter and the HBCLLC converter are shown in Fig. 6(a) and (b), respectively.

For FBCLLC circuit, the parameters will be derived as:

$$\begin{aligned} R_{e,FB}' &= (8/n^2\pi^2)R_o' \quad & L_1' &= L_1/n^2 \\ C_1' &= n^2 C_1 \quad & L_m' &= L_m/n^2 \end{aligned} \tag{8}$$

Similarly, for HBCLLC circuit, they are derived as follows:

$$\begin{aligned} R_{e,HB}' &= (2/n^2\pi^2)R_o' \quad & L_1' &= L_1/n^2 \quad & C_1' &= C_{11}' + C_{12}' \\ C_2 &= C_{21} + C_{22} \quad & C_{11}' &= n^2 C_{21} \quad & C_{12}' &= n^2 C_{22} \\ L_m' &= L_m/n^2 \end{aligned} \tag{9}$$

The gain of the converter in discharging mode is derived as follows:

$$G_{CLLC,V2G} = n \cdot \frac{1}{\sqrt{c^2 + d^2}} \tag{10}$$

where,

$$c = \frac{1}{h'} + 1 - \frac{1}{h' \cdot \omega'^2} \tag{11}$$

$$d = \left(\frac{k'}{h'} + 1 + \frac{1}{g' \cdot h'} + \frac{1}{g'}\right)\frac{Q'}{\omega'} - \left(\frac{k'}{h'} + 1 + k'\right)Q' \cdot \omega' - \frac{Q'}{g' \cdot h' \cdot \omega'^3} \tag{12}$$

$$\begin{cases} h' = \frac{L_m'}{L_2}, k' = \frac{L_1'}{L_2}, g' = \frac{C_1'}{C_2}, \omega' = \frac{\omega_s}{\omega_r'} \\ \omega_r' = \frac{1}{\sqrt{L_2 C_2}}, Q' = \frac{\sqrt{L_2/C_2}}{R_e'} \end{cases} \tag{13}$$

With the same L and C values, the ω_r', k', g', and h' of both FBCLLC and HBCLLC circuits will maintain the same values as the ω_r, k, g, and h in charging mode, respectively. However, Q' will change since the equivalent load changes. Q' can be calculated as:

$$Q' = n^2 R_o / R_o' Q \tag{14}$$

3) Soft-switching Region

Fig. 5 shows the inductive and capacitive resonate network regions of the CLLC circuit. The resonant network is inductive when the slope of the gain is negative. ZVS can be realized in inductive region. To ensure the primary switches turn on with ZVS, the magnetizing inductor current should be large enough to fully charge/discharge the output capacitors of the MOSFETs during the dead band time. The maximum value of L_m for a FBCLLC converter is derived in [17] as follows:

$$L_{m,FB} \leq \frac{t_{db}}{16 C_{oss} f_{s,max}} \tag{15}$$

Similarly, for a HBCLLC converter, the L_m can be calculated as:

$$L_{m,HB} \leq \frac{t_{db}}{8 C_{oss} f_{s,max}} \tag{16}$$

where, t_{db} is the dead band time duration, C_{oss} is the output capacitance of the MOSFET, and $f_{s,max}$ is the maximum switching frequency.

B. Bidirectional DAB converters

1) Operating Principles

Typical steady-state waveforms of a FBDAB converter (shown in Fig. 2(a)) with single-phase-shift control at heavy load conditions are shown in Fig. 7(a). It has been assumed that $V_{in}/n < V_o$ and $i_L(t_a) < 0$. T_s is the switching period, and $T_s = 1/f_s$, where f_s is the switching frequency. The phase-shift between the two bridges, t_{shift}, is $DT_s/2$, and D is from 0 to 0.5. v_1 is the voltage on the secondary side of the transformer, and v_2 is the input voltage of the rectifier. v_L is the voltage across the inductor, L, therefore, $v_L = v_1 - v_2$. i_L is the inductor current. Prior to t_a, Q_2, Q_3, Q_5 and Q_8 are on, and Q_1, Q_4, Q_6 and Q_7 are off. At t_a, Q_1 and Q_4 turn on, Q_2 and Q_3 turn off. t_{shift} later, Q_6 and Q_7 turn on, Q_5 and Q_8 turn off. i_L is negative at t_a and positive at t_b, which means Q_1, Q_4, Q_6 and Q_7 turn on with ZVS. However, in light load conditions, i_L may be positive at t_a and negative at t_b, as shown in Fig. 7(b), which means ZVS cannot be achieved. Detailed analysis can be found in [20]. The other half cycle has similar operating modes but with opposite current direction. The HBDAB circuit has similar waveforms with half inductor voltage.

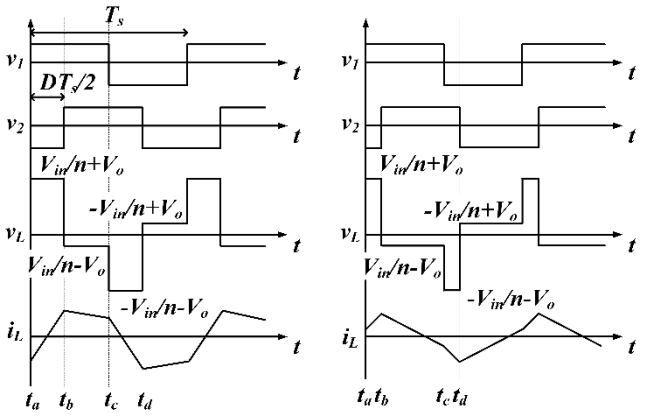

Fig. 7. Typical waveforms of a FBDAB converter for $V_{in}/n < V_o$ and $i_L(t_a) < 0$ in (a) heave load condition, (b) light load condition.

2) Gain Analysis

Based on the analysis in [20], the gain of the FBDAB converter can be calculated as:

$$G_{FBDAB,G2V} = \frac{V_{out}}{V_{in}} = \frac{1}{n} \cdot \frac{R_o}{2 f_s L} D(1-D) \tag{17}$$

The output power is derived as

$$P_{FBDAB,G2V} = \frac{V_{in} V_{out}}{2 n f_s L} D(1-D) \tag{18}$$

Similarly, the gain and output power of the HBDAB can be derived respectively as follows:

$$G_{HBDAB,G2V} = \frac{1}{n} \cdot \frac{R_o}{8 f_s L} D(1-D) \tag{19}$$

$$P_{HBDAB,G2V} = \frac{V_{in} V_{out}}{8 n f_s L} D(1-D) \tag{20}$$

In discharging mode, the gain and output power of the FBDAB can be derived respectively as follows:

$$G_{FBDAB,V2G} = \frac{1}{n} \cdot \frac{R_o'}{2 f_s L} D(1-D) \tag{21}$$

$$P_{FBDAB,V2G} = \frac{V_{in} V_{out}}{2 n f_s L} D(1-D) \tag{22}$$

For the HBDAB circuit,

$$G_{HBDAB,V2G} = \frac{1}{n} \cdot \frac{R_o'}{8 f_s L} D(1-D) \tag{23}$$

$$P_{HBDAB,V2G} = \frac{V_{in} V_{out}}{8 n f_s L} D(1-D) \tag{24}$$

3) Soft-switching Region

According to the analysis, to ensure fully ZVS operation, the inductor current is required to be negative at t_a ($i_L(t_a) \leq 0$), and positive at t_b ($i_L(t_b) \geq 0$). The requirements of phase-shift D can be calculated as follows [20]:

$$\begin{cases} D \geq \frac{G_{DAB}-1}{2 G_{DAB}} & \text{if } G_{DAB} \geq 1 \\ D \geq \frac{1-G_{DAB}}{2} & \text{if } G_{DAB} \leq 1 \end{cases} \tag{25}$$

Equation (25) can be applied to the HBDAB circuit as well. Based on (25), the ZVS region of both FBDAB and HBDAB

converters is shown in Fig. 8. The converters can always operate under ZVS condition when the gain is $1/n$. Otherwise, with lowering the phase-shift, the ZVS region of the converter decreases. Therefore, in light conditions, since the phase-shift must be smaller to maintain the gain, the converters may lose soft-switching, which will cause large switching losses.

III. Design Methodology

In charging mode, the input voltages of all four topologies are 500 V, and the output voltage range is 200 - 420 V. For discharging mode, the input voltage range is 350 – 420 V, and the output voltage is 500 V. The nominal operating frequency for both charging and discharging modes is 170 kHz.

A. Bidirectional CLLC converters

For the CLLC converters, the transformer turns ratio n is set to be 1.5 in order to step down the input voltage and simplify the control. The G2V gain, therefore, can be designed to be $0.6/n$ - $1.3/n$, and the V2G gain range should be wider than $0.79n$ - $0.96n$. Furthermore, the curve of the two gains should decrease monotonically in the designed zone for linear control. From Fig. 6, a larger Q can give a narrower operating frequency range, whereas a smaller Q can guarantee the gain and the monotony of the gain. In this design, $Q = 0.4$ is chosen for full load condition ($R_o = 176\ \Omega$) in charging mode and the resonant frequency f_r is designed to be 170 kHz. For a simplified design, C_1 is equal to C_2', and L_1 is equal to L_2'. The relation between Q and L_m is given in [28]. Large L_m reduces the peak current, which lowers conduction loss, but it will also reduce the gain of the circuit. Furthermore, from (15) and (16), larger L_m may cause hard switching of the power MOSFETs. Therefore, considering the trade-off between gain and conduction loss, L_m is chosen to be four times larger than L_1. Hence, L_1, L_2, L_m, C_1 and C_2, for the FBCLLC circuit can be calculated from (5) and (6), which will lead to,

$$\begin{cases} L_1 = 120.2\ \mu H, L_2 = 53.4\ \mu H \\ C_1 = 7.3\ nF, C_2 = 16.4\ nF \\ L_m = 480.8\ \mu H \end{cases} \tag{26}$$

Similarly, the parameters for the HBCLLC circuit can be calculated from (5) and (7) as follows:

$$\begin{cases} L_1 = 30.1\ \mu H, L_2 = 13.4\ \mu H \\ C_{11} = C_{12} = 14.6\ nF, C_{21} = C_{22} = 32.8\ nF \\ L_m = 120.4\ \mu H \end{cases} \tag{27}$$

Fig. 9 illustrates the gains of charging and discharging modes for both FBCLLC and HBCLLC circuits with the parameters calculated above, which satisfy the design requirements.

B. Bidirectional DAB converters

Equations (17) and (21) show that the transformer turns ratio n has the same effect on the gains of DAB circuit in both charging and discharging modes. For example, if $n > 1$, the transformer will help step down the voltage in charging mode, however, in discharging mode, the transformer will still step down the voltage. In this design, the transformer turns ratio n is set to be 1.5 to balance the control pressure in both power flows and fully use the ZVS region shown in Fig. 8. The G2V gain, hence, can be designed to be $0.6/n$ - $1.3/n$, and the V2G gain

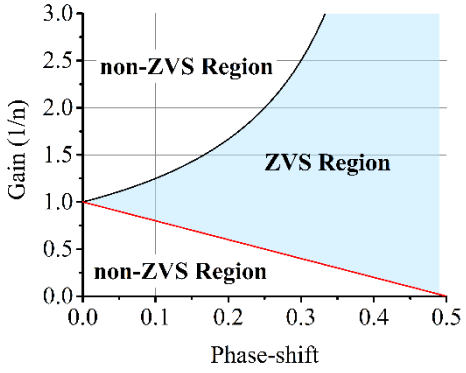

Fig. 8. ZVS region of DAB converters.

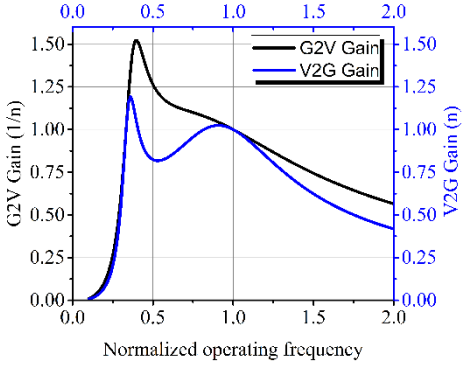

Fig. 9. The gains of the CLLC circuits in charging and discharging modes.

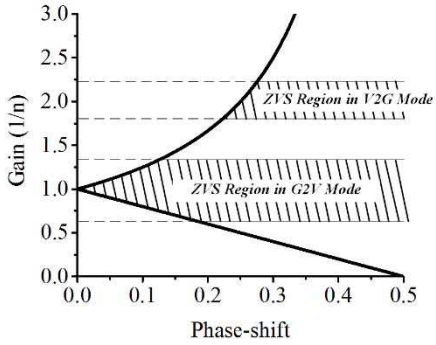

Fig. 10. Full ZVS regions of the DAB converters in both charging and discharging modes.

range should be wider than $1.7/n$ - $2.2/n$. The operating frequency f_s of this circuit is 170 kHz. To reduce the reactive power [26] and make the gain more linear, the maximum phase-shift D_{max} is set to be 0.45 for the worst case. Since the system cannot operate with full power when $V_o = 200$ V for battery charging, the worst case happens in discharging mode with $V_{in} = 350$ V, $V_o = 500$ V, and $P = 1$ kW.

For the FBDAB circuit, the inductance L, therefore, can be calculated from (22):

$$L_{FBDAB} = \frac{V_{in}V_{out}}{2nf_sP} D_{max}(1 - D_{max}) = 84.9\ \mu H \tag{28}$$

Similarly, for the HBDAB circuit, the inductance L can be calculated from (24):

$$L_{HBDAB} = \frac{V_{in}V_{out}}{8nf_sP} D_{max}(1 - D_{max}) = 21.2\ \mu H \tag{29}$$

From (25), the minimum phase-shift can be calculated for each gain. In this design, for both FBDAB and HBDAB converters, the full ZVS regions in both charging and discharging modes are shown in the shadow areas in Fig. 10. At light loads, the phase-shift is reduced to maintain the gain; however, in this condition, the converters lose ZVS.

IV. Experimental Results

Fig. 11 illustrates the experimental setup for testing the prototypes. The components of the CLLC and DAB circuits are listed in Table I and Table II, respectively.

The switches are SiC power MOSFETs, which have high voltage and current ratings with low output capacitance. A TMS320F28335 DSP-based digital control platform is used to generate the control signal for the circuits. Since the magnetizing inductance L_m of the transformer in the FBCLLC circuit is higher than that in the HBCLLC circuit, the transformer in the FBCLLC circuit requires more number of turns to ensure higher magnetizing inductance.

Fig. 12 shows the four prototypes. Since the four converters have similar topologies and for simplicity as well as rapid prototyping, the converters are tested based on one general PCB platform. The film capacitors in CLLC converters are connected in parallel to reduce ESR. Other two bridge capacitors are connected on the bottom of the HBDAB board.

Fig. 13(a) and (b) illustrate the experimental waveforms of the FBCLLC and the HBCLLC circuits in charging mode. The load is 800 W, $V_o = 300$ V and $f_s = 200$ kHz. It is clear that, for each of the circuits, the switches turn on with ZVS. The circuits have similar experimental results in discharging mode since the structures of the circuits are symmetrical.

Fig. 14(a) and (b) show the FBDAB and the HBDAB circuits experimental waveforms in charging mode at phase-shift $D = 0.4$, respectively. The load is 800 W, $V_o = 300$ V and $f_s = 170$ kHz. In this case, $V_o < V_{in}/n$. The waveforms show that the switches turn on with ZVS. Similar experimental results are obtained in discharging mode.

Fig. 15 shows an example at light load condition. The HBCLLC and HBDAB converters operate at 100 V output voltage and 50 W load condition. Since the CLLC converter is controlled through frequency modulation and the DAB converter is controlled through phase-shift modulation, the operating frequency is 500 kHz for HBCLLC converter and remains 170 kHz for the HBDAB converter. The phase-shift D of the HBCLLC converter is set to be 0.1 for this light load condition. It is clear that the switch of the HBCLLC converter still operates with ZVS, whereas the secondary side switch of the HBDAB converter loses ZVS. The experimental results verify the previous analysis.

Fig. 16(a) and (b) show the efficiencies of the four circuits in charging and discharging modes, respectively. The output voltage is 300 V for charging mode and 500 V for discharging mode.

V. Experimental Results Analysis

Summaries of the comparisons are presented in Table III and Fig. 17.

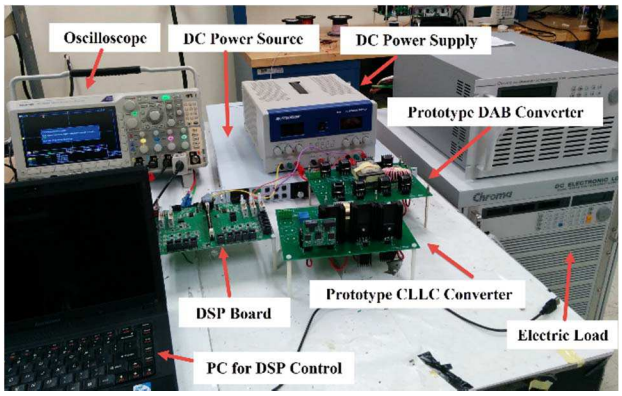

Fig. 11. Experimental setup to test the prototypes.

TABLE I
THE COMPONENTS OF CLLC CONVERTERS

FBCLLC		HBCLLC	
Component	Product/Value	Component	Product/Value
S_1- S_8	C2M0080120D	S_1, S_2, S_7, S_8	C2M0080120D
n	18:12	n	12:8
L_m	522 μH	L_m	131 μH
L_1	131 μH	L_1	32 μH
L_2	60 μH	L_2	15 μH
C_1	7.8 nF	C_{11}, C_{12}	14.2 nF
C_2	17.0 nF	C_{21}, C_{22}	33.0 nF

TABLE II
THE COMPONENTS OF DAB CONVERTERS

FBCLLC		HBCLLC	
Component	Product/Value	Component	Product/Value
Q_1- Q_8	C2M0080120D	Q_1, Q_2, Q_7, Q_8	C2M0080120D
n	12:8	n	12:8
L	90 μH	L	22 μH
		C_{11}, C_{12}, C_{21}, C_{22}	30 μF

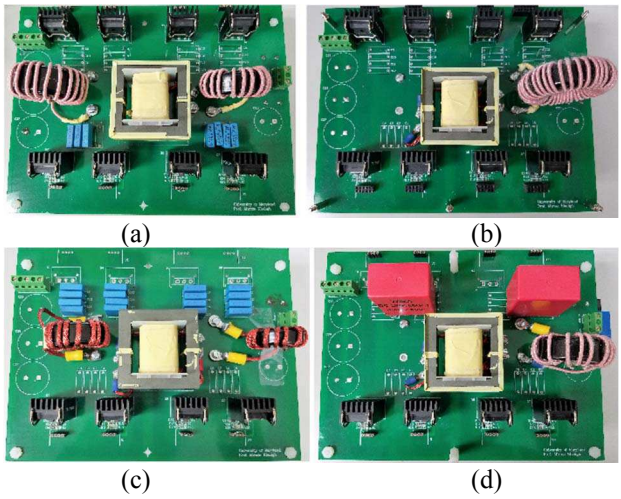

Fig. 12. Different DC-DC converter prototypes: (a) FBCLLC, (b) FBDAB, (c) HBCLLC, (d) HBDAB.

A. Efficiency

From the experimental results, all the circuits achieve high efficiency. The highest efficiencies in charging mode are 95.0% and 96.5% for the FBCLLC and the HBCLLC circuits respectively, and 96.1% and 97.4% in discharging mode. The

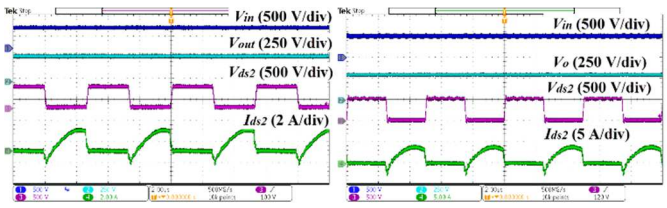

Fig. 13. Experimental waveforms of (a) the FBCLLC circuit and (b) the HBCLLC circuit at $load = 800$ W, $V_o = 300$ V, and $f_s = 200$ kHz.

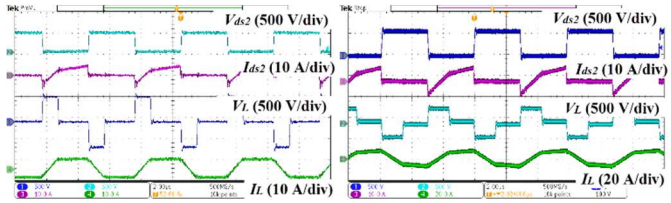

Fig. 14. Experimental waveforms of (a) the FBDAB circuit and (b) the HBDAB circuit at $load = 800$ W, $V_o = 300$ V, $f_s = 170$ kHz, and $D = 0.4$.

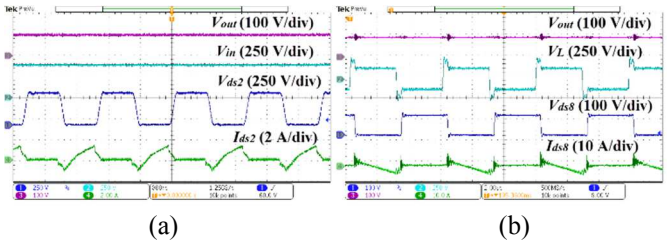

Fig. 15. Experimental waveforms of (a) the HBCLLC circuit and (b) the HBDAB circuit at $load = 50$ W, and $V_o = 100$ V.

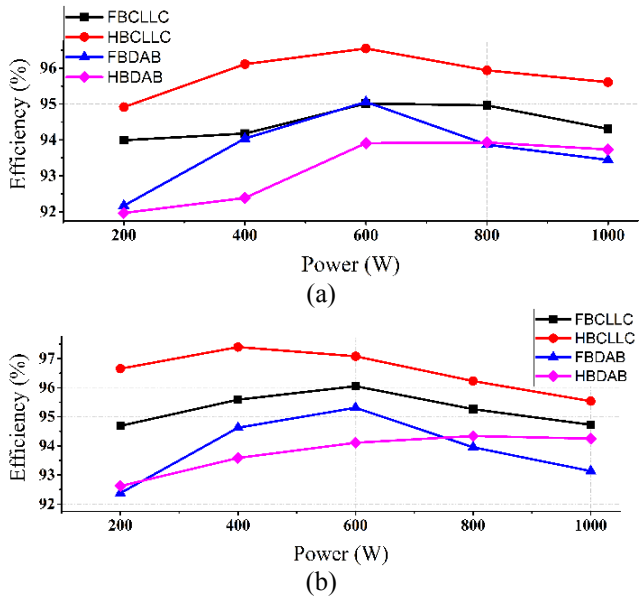

Fig. 16. Measured efficiency of the four circuits in (a) charging and (b) discharging modes.

highest efficiencies are achieved when the circuits operate closed to the resonant frequency. When the operating frequency is much smaller or larger than the resonant frequency, the circulating loss will increase and reduce the efficiency. For the

TABLE III
THE COMPARISON OF THE CONVERTERS

	FBCLLC	HBCLLC	FBDAB	HBDAB
Soft-switching Region	Full load	Full load	Partial load	Partial load
Control Modulation	Frequency	Frequency	Phase-shift	Phase-shift
Design Complexity	High	High	Low	Low

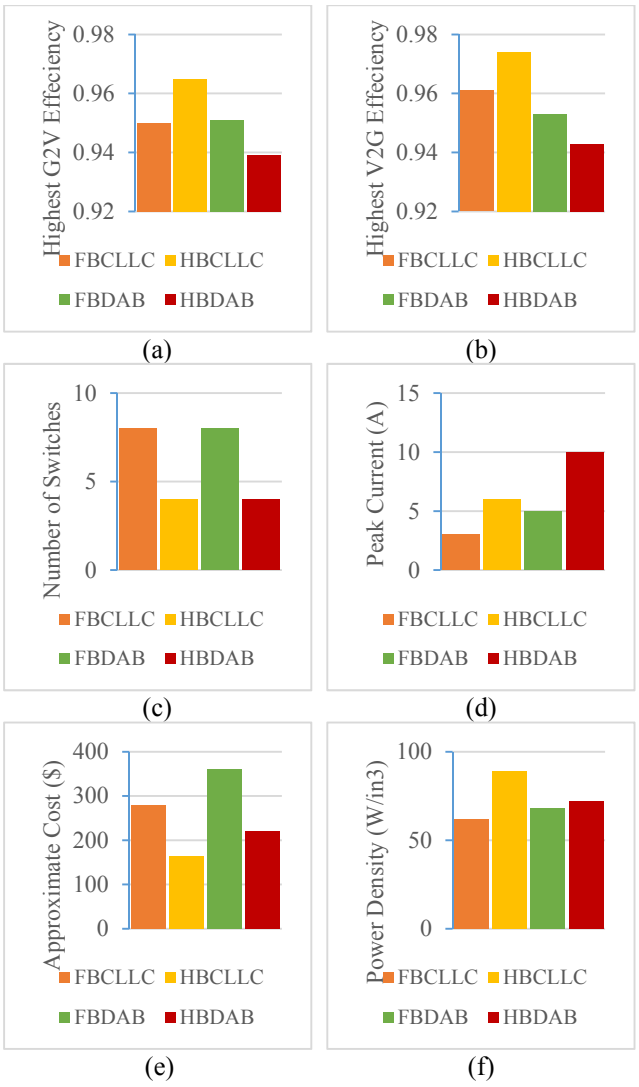

Fig. 17. Comparison for (a) Highest G2V efficiency, (b) Highest V2G efficiency, (c) Number of switches, (d) Peak current of switch, (d) Approximate cost of each converter, and (f) Power density.

FBDAB and the HBDAB circuits, the highest efficiencies are 95.1% and 93.9% in charging mode, and 95.3% and 94.3% in discharging mode, respectively. The efficiencies of the CLLC circuits are higher than those of the DAB circuits, since the switches of the DAB circuits loss ZVS at light load conditions, and the SPS control strategy creates relatively large reactive power in the circuits which also reduces the efficiency.

In addition, comparing to the full-bridge structure, the half-bridge structure helps the circuits improves the overall efficiency, due to the reduction of the total number of switches and corresponding driving circuits. An extra benefit of the half-

bridge structure of the resonant converters is that the two capacitors in each leg can automatically reduce flux imbalance for the transformer.

B. Soft-switching Region

From the analysis in Section II, the soft-switching region of the CLLC circuits are much wider than that of the DAB circuits especially at light load conditions. With an appropriate design, both FBCLLC and HBCLLC converters can achieve full soft-switching in the entire load range. However, for DAB converters, Fig. 10 and Fig. 15 show that the converters lose ZVS at light load conditions. Therefore, it is difficult to maintain soft-switching of all the switches for wide load range. Furthermore, for CLLC circuits, lighter loads provide wider soft-switching regions, whereas for DAB circuits, it is opposite.

C. Design and Control Complexity

According to the analysis in Section II, if the CLLC circuits operate closed to their resonant frequencies, the gains will be about $1/n$, independent of the loads. Therefore, if the operating frequency can be adjusted at the vicinity of the resonant frequency, both FBCLLC and HBCLLC circuits are perfect for constant output voltage, variable load conditions. However, the gains of the CLLC circuits are non-linear with the loads. Furthermore, depending on the value of Q and particularly at small Q values, the required operating frequency range will be very large. Hence, in the case of a wide output voltage range, the value of Q should be carefully chosen to limit the operating frequency range.

In the case of the DAB circuits, the gains are proportional to the loads, and almost linearly related to the phase-shift when $D \leq 0.45$. Therefore, comparing the DAB converters to the CLLC converters, the design and control complexity for the DAB converters is less.

D. Component Selection

For the CLLC converter, the output current is sinusoidal, whereas for the DAB converter, the output current has more high order harmonic ripples than that of the CLLC converter. Therefore, an extra current filter may be needed for the DAB circuits.

Comparing the full-bridge and the half-bridge structures, under the same input and output conditions, in the half-bridge structure, both primary side and secondary side currents are twice larger than those in the full-bridge structure. Therefore, the switches, resonant components and transformer of the half-bridge converters are under about twice larger current stress than those of the full-bridge converters.

E. Power Density

It is clear that, with reducing the number of switches, the half-bridge structure has benefits in terms of size and weight, since the number of corresponding driving circuits and cooling systems can be reduced at the same time. Furthermore, with the same gain, the half-bridge structure requires less inductance than the full-bridge structure. Therefore, the size of the converters with half-bridge structure should be smaller than that with full-bridge structure. Comparing the two half-bridge converters, HBCLLC and HBDAB converters, although the HBCLLC converter requires one more inductor, the bridge capacitances of the HBCLLC converter are much smaller than those of the HBDAB converter, since they are also used as resonant capacitors. Therefore, in this comparison, the size and weight of the HBCLLC circuit is less than those of the other circuits, which means the power density of the HBCLLC circuit is the highest. Furthermore, the SiC MOSFETs and their gate drivers cost the most in the converters, and reducing number of switches will reduce the cost of the converters. Therefore, the half-bridge converters cost less than the full-bridge converters.

VI. Conclusions

This manuscript provides a comprehensive analysis of and comparison among the FBCLLC, HBCLLC, FBDAB, and HBDAB converters for EV battery charging applications. A new general gain expression of the HBCLLC converter is derived in this manuscript. The practicability and performance of the four DC-DC converters for bidirectional EV charging systems are discussed. The converters are designed with 1 kW power rating. All the converters can achieve high efficiency and bidirectional power flow. The topologies, operating principles and design methodologies of the converters are discussed, and the performances of the converters are compared. Although the current stress on the HBCLLC converter is relatively high, the power density of the HBCLLC converter is the highest and the cost is relatively low. Soft-switching can be achieved in full load range for HBCLLC converter, and in addition, if the input voltage could be adjustable, the HBCLLC converter can be operated at the resonant frequency which is with highest efficiency. Therefore, for bidirectional, wide load EV charging systems, the CLLC converters are slightly better than DAB converters. Considering the efficiency, size and cost, the HBCLLC converter will be the most suitable choice at 1kW.

References

[1] A. S. O. Yu, L. L. C. Silva, C. L. Chu, P. T. S. Nascimento and A. S. Camargo, "Electric vehicles: Struggles in creating a market," in *Proc. IEEE PICMET*, Jul. 2011, pp. 1–13.

[2] B. Whitaker et al., "A high-density, high-efficiency, isolated on-board vehicle battery charger utilizing silicon carbide power devices," *IEEE Trans. Power Electron.*, vol. 29, no. 5, pp. 2606–2617, May 2014.

[3] I. O. Lee and G. W. Moon, "Half-bridge integrated ZVS full-bridge converter with reduced conduction loss for electric vehicle battery chargers," *IEEE Trans. Ind. Electron.*, vol. 61, no. 8, pp. 3978–3988, Aug. 2014.

[4] B. Gu, J. S. Lai, N. Kees and C. Zheng, "Hybrid-switching full-bridge DC–DC converter with minimal voltage stress of bridge rectifier, reduced circulating losses, and filter requirement for electric vehicle battery chargers," *IEEE Trans. Power Electron.*, vol. 28, no. 3, pp. 1132–1144, Mar. 2013

[5] A. Emadi, Y. J. Lee and K. Rajashekara, "Power electronics and motor drives in electric, hybrid electric, and plug-in hybrid electric vehicles," *IEEE Trans. Ind. Electron.*, vol. 55, no. 6, pp. 2237–2245, Jun. 2008.

[6] C. A. Gallo, F. L. Tofoli and J. A. C. Pinto, "A passive lossless snubber applied to the AC–DC interleaved boost converter," *IEEE Trans. Power Electron.*, vol. 25, no. 3, pp. 775–785, Mar. 2010.

[7] M. Pahlevaninezhad, P. Das, J. Drobnik, P. K. Jain and A. Bakhshai, "A ZVS interleaved boost AC/DC converter used in plug-in electric vehicles," *IEEE Trans. Power Electron.*, vol. 27, no. 8, pp. 3513–3529, Aug. 2012.

[8] S. M. Lukic, J. Cao, R. C. Bansal, F. Rodriguez and A. Emadi, "Energy storage systems for automotive applications," *IEEE Trans. Ind. Electron.*, vol. 55, no. 6, pp. 2258–2267, Jun. 2008.

[9] H. Wang, S. Dusmez and A. Khaligh, "Maximum efficiency point tracking technique for LLC-based PEV chargers through variable DC link

control," *IEEE Trans. Ind. Electron.*, vol. 61, no. 11, pp. 6041–6049, Nov. 2014.
[10] J. Deng, S. Li, S. Hu, C. C. Mi and R. Ma, "Design methodology of LLC resonant converters for electric vehicle battery chargers," *IEEE Trans. Veh. Technol.*, vol. 63, no. 4, pp. 1581–1592, May 2014.
[11] B. Kramer, S. Chakraborty, and B. Kroposki, "A review of plug-in vehicles and vehicle-to-grid capability," in *Proc. IEEE IECON*, Nov. 2008, pp. 2278–2283.
[12] U. K. Madawala and D. J. Thrimawithana, "A bidirectional inductive power interface for electric vehicles in V2G systems," *IEEE Trans. Ind. Electron.*, vol. 58, no. 10, pp. 4789–4796, Oct. 2011.
[13] M. H. Ryu, H. S. Kim, J. W. Baek, H. G. Kim and J. H. Jung, "Effective test bed of 380-V DC distribution system using isolated power converters," *IEEE Trans. Ind. Electron.*, vol. 62, no. 7, pp. 4525–4536, Jul. 2015.
[14] Z. U. Zahid, Z. M. Dalala, R. Chen, B. Chen and J. S. Lai, "Design of bidirectional DC–DC resonant converter for vehicle-to-grid (V2G) applications," *IEEE Trans. Transp. Electrification*, vol. 1, no. 3, pp. 232–244, Oct. 2015.
[15] L. Xue, Z. Shen, D. Boroyevich, P. Mattavelli and D. Diaz, "Dual active bridge-based battery charger for plug-in hybrid electric vehicle with charging current containing low frequency ripple," *IEEE Trans. Power Electron.*, vol. 30, no. 12, pp. 7299–7307, Dec. 2015.
[16] W. Chen, P. Rong, and Z. Lu, "Snubberless bidirectional DC-DC converter with new CLLC resonant tank featuring minimized switching loss," *IEEE Trans. Ind. Electron.*, vol. 57, no. 9, pp. 3075–3086, Sep. 2010.
[17] J. H. Jung, H. S. Kim, M. H. Ryu, and J. W. Baek, "Design methodology of bidirectional CLLC resonant converter for high-frequency isolation of DC distribution systems," *IEEE Trans. Power Electron.*, vol. 28, no. 4, pp. 1741–1755, Apr. 2013.
[18] F. Lu, H. Zhang, H. Hofmann and C. Mi, "A CLLC-compensated high power and large air-gap capacitive power transfer system for electric vehicle charging applications," in *Proc. IEEE APEC*, Mar. 2016, pp. 1721–1725.
[19] X. Yan, H. Zhao, Q. Zhang, H. Liu, and Z. Lv, "An efficient isolated bidirectional half bridge resonant DC/DC converter," in *Proc. IEEE ICSET*, Sep. 2012, pp. 48–53.
[20] C. Mi, H. Bai, C. Wang, and S. Gargies, "Operation, design and control of dual h-bridge-based isolated bidirectional DC-DC converter," *IET Power Electron.*, vol. 1, no. 4, pp. 507–517, Dec. 2008.
[21] D. K. Jeong, M. H. Ryu, H. G. Kim, and H. J. Kim, "Optimized design of bi-directional dual active bridge converter for low-voltage battery charger," *J. Power Electron.*, vol. 14, no. 3, pp. 468–477, May 2014.
[22] L. Xue, D. Boroyevich and P. Mattavelli, "Switching condition and loss modeling of GaN-based dual active bridge converter for PHEV charger," in *Proc. IEEE APEC*, Mar. 2016, pp. 1315–1322.
[23] T. Ngo, J. Won and K. Nam, "A single-phase bidirectional dual active half-bridge converter," in *Proc. IEEE APEC*, Feb. 2012, pp. 1127–1133.
[24] H. Higa, S. Takuma, K. Orikawa and J. I. Itoh, "Dual active bridge DC-DC converter using both full and half bridge topologies to achieve high efficiency for wide load," in *Proc. IEEE ECCE*, Sep. 2015, pp. 6344–6351.
[25] B. Zhao, Q. Song, W. Liu, and Y. Sun, "Overview of dual-active-bridge isolated bidirectional DC-DC converter for high-frequency-link power conversion system," *IEEE Trans. Power Electron.*, vol. 29, no. 8, pp. 4091–4106, Aug. 2014.
[26] H. Bai and C. Mi, "Eliminate reactive power and increase system efficiency of isolated bidirectional dual-active-bridge DC/DC converters using novel dual-phase-shift control," *IEEE Trans. Power Electron.*, vol. 23, no. 6, pp. 2905–2914, Nov. 2008.
[27] B. Zhao, Q. Yu and W. Sun, "Extended-phase-shift control of isolated bidirectional DC-DC converter for power distribution in microgrid," *IEEE Trans. Power Electron.*, vol. 27, no. 11, pp. 4667–4680, Nov. 2012.
[28] B. Lu, W. Liu, Y. Liang, F. C. Lee, and J. D. van Wyk, "Optimal design methodology for LLC resonant converter," in *Proc. IEEE APEC*, Mar. 2006, pp. 6–12.

Peiwen He received the B.S. degree with honor from Zhejiang University, Hangzhou, China, in 2010 and the M.S. degree from Illinois Institute of Technology, Chicago, in 2012 both in Electrical Engineering. He is currently working toward the Ph.D. degree in the Electrical and Computer Engineering Department at the University of Maryland, College Park.

Since 2015, he has been working as a graduate research assistant in the Maryland Power Electronics Laboratory (MPEL). His research interests include modeling and design of high-frequency AC-DC, DC-DC and DC-AC power electronic converters and electric chargers for PEV. Currently, he is working on developing a high-frequency integrated, isolated and bi-directional on-board charger for PEV.

Alireza Khaligh (S'04, M'06, SM'09) is an Associate Professor at the Electrical and Computer Engineering (ECE) Department and the Institute for Systems Research (ISR) in the University of Maryland (UMD). His major research interests include modeling, analysis, design, and control of power electronic converters for transportation electrification, renewable energies, energy harvesting, and microrobotics. He is an author/coauthor of over 160 journal and conference papers. Dr. Khaligh is an Associate Editor of the IEEE Transactions on Power Electronics (TPEL), and an Associate Editor for IEEE Transactions on Transportation Electrification.He was a Guest Associate Editor for the Special Issue of IEEE TPEL on Transportation Electrification and Vehicle Systems, and a Guest Editor for the Special Section of IEEE Transactions on Vehicular Technology on Sustainable Transportation Systems.

Dr. Khaligh is a recipient of various awards and recognitions including the 2016 Junior Faculty Outstanding Research Award from Clark School of Engineering at UMD, 2015 Inaugural ISR Junior Faculty Fellowship from the Institute for Systems Research at UMD, the 2013 George Corcoran Memorial Award from the ECE Department at UMD, 2010 Ralph R. Teetor Educational Award from the Society of Automotive Engineers, 2009 Armour College of Engineering Excellence in Teaching Award from Illinois Institute of Technology, and three prize transaction paper awards. Dr. Khaligh was the General Chair of the 2016 IEEE Applied Power Electronic Conference and Expo (APEC), Long Beach, CA, and also the General Chair of the 2013 IEEE Transportation Electrification Conference and Expo (ITEC), Dearborn, MI. He is a Distinguished Lecturer of the IEEE Industry Applications Society and IEEE Vehicular Technology Society.